

Backward Joint Model for Dynamic Prediction using Multivariate Longitudinal and Competing Risk Data

Wenhao Li¹, Liang Li^{1,*}, Brad C. Astor², Wei Yang³, Tom H. Greene⁴

¹ Department of Biostatistics, The University of Texas MD Anderson Cancer Center, Houston, TX, U.S.A.

² School of Medicine and Public Health, University of Wisconsin-Madison, Madison, WI, U.S.A.

³ Perelman School of Medicine, University of Pennsylvania, Philadelphia, PA, U.S.A.

⁴ School of Medicine, University of Utah, Salt Lake City, UT, U.S.A.

* *email*: LLi15@mdanderson.org

Abstract

Joint modeling is a useful approach to dynamic prediction of clinical outcomes using longitudinally measured predictors. When the outcomes are competing risk events, fitting the conventional shared random effects joint model often involves intensive computation, especially when multiple longitudinal biomarkers are used as predictors, as is often desired in prediction problems. Motivated by a longitudinal cohort study of chronic kidney disease, this paper proposes a new joint model for the dynamic prediction of end-stage renal disease with the competing risk of death. The model factorizes the likelihood into the distribution of the competing risks data and the distribution of longitudinal data given the competing risks data. The estimation with the EM algorithm is efficient, stable and fast, with a one-dimensional integral in the E-step and convex optimization for most parameters in the M-step, regardless of the number of longitudinal predictors. The model also comes with a consistent albeit less efficient estimation method that can be quickly implemented with standard software, ideal for model building and diagnostics. This model enables the prediction of future longitudinal data trajectories conditional on being at risk at a future time, a practically significant problem that has not been studied in the statistical literature. We study the properties of the proposed method using simulations and a real dataset and compare its performance with the shared random effects joint model.

Keywords: Competing risks; Dynamic prediction; Joint model; Multivariate longitudinal data; Survival analysis.

1 Introduction

Chronic kidney disease (CKD) is a major public health burden, affecting approximately 14% of the adult population in the US. It is characterized by a gradual and often irreversible deterioration of kidney function that may occur over years (Appel et al., 2023). The stages of CKD are defined based on kidney function, usually quantified by the glomerular filtration rate (GFR, in mL/min/1.73 m²). GFR estimates how well the kidneys filter waste and excess fluid from the blood. Stages 1, 2, 3A, 3B, 4 and 5 correspond to GFR in ≥ 90 , $60 - 89$, $45 - 59$, $30 - 44$, $15 - 29$, and < 15 mL/min/1.73 m², respectively. At stage 5, patients need to be prepared for entering End-Stage Renal Disease (ESRD), when the kidneys stop functioning adequately and either dialysis or kidney transplant is required to sustain life. More severe CKD is progressively associated with many adverse outcomes, including cardiovascular disease, stroke, heart failure and peripheral vascular disease (Appel et al., 2023). Major causes of CKD in the US include diabetes mellitus and hypertension. CKD, aging, and these comorbidities may result in death, though the exact cause can be difficult to ascertain and is often multifactorial.

Predicting ESRD is important for CKD research, patient counseling, and clinical management of the disease. Various prediction models have been proposed (Lim et al., 2022), but they leave one or more of statistical challenges unaddressed. First, the prediction should ideally adapt to the ever-changing at-risk population and the potentially time-varying association between the predictor and outcome (Li et al., 2016). The at-risk population changes because of both aging and systematic differences between those who progress to ESRD early and those who do not. The relative importance of predictors may vary at various stages of the disease. Second, it is important to have the capacity to incorporate prior clinical history into prediction, as opposed to only the current health status. Third, the prediction of ESRD should adjust for the competing risk by death to avoid bias and produce proper interpretation. Fourth, not all patients are equally concerned about the near-future risk of ESRD. Those at earlier stages have low ESRD risk and are more interested in the future progression trajectory of GFR if ESRD or death does not occur (GFR is undefined when a patient reaches ESRD or death, obviously).

The statistical challenges above can be handled in the framework of dynamic prediction (Taylor et al., 2005; Yu et al., 2008; Rizopoulos, 2011). A typical approach is to estimate the conditional joint distribution of the longitudinal predictor variables (e.g., GFR) and survival data (e.g., the times of ESRD and death), given the time-invariant predictors. Once this joint distribution is estimated from the training dataset, the prediction for any subject in the validation dataset can be calculated straightforwardly from the conditional distribution given the longitudinal history before the prediction time. Therefore, the key to dynamic prediction is to build an appropriate joint model of longitudinal and survival data. Comprehensive reviews on this topic are available (Rizopoulos, 2012; Elashoff et al., 2016; Andrinopoulou et al., 2021), but the published statistical methods are insufficient to study the aforementioned CKD problem.

First, most published joint modeling research presented data applications and simulations with a very small number of longitudinal variables. The main reason is that the likelihood function of these models is complicated and contains an analytically intractable numerical integration for each of the n subjects in the training dataset. Since the typical joint model uses shared random effects to quantify the association between longitudinal and

survival data, the dimension of the integral increases linearly with the number of longitudinal variables, and the number of unknown parameters in the random effects distribution increases quadratically. In addition, the marginal log-likelihood function is usually not concave with multiple local maxima, which may cause non-convergence or computational instability in numerical optimization, especially when the number of unknown parameters is large. These are widely recognized difficulties in the implementation of such models. (Rizopoulos, 2012; Elashoff et al., 2016) They become particularly troublesome when we use joint models for prediction problems, which may require a large number of longitudinal predictors for improved predictive accuracy. Second, the aforementioned computational problem exacerbates the joint modeling with competing risk outcomes, whose multiple survival endpoints further increase the number of shared random effects. The limited literature on this topic presented numerical studies with a small number of random effects (or dimension of integrals), typically coming from one or two longitudinal variables, and with “brute force” maximum likelihood or Bayesian computation to tackle the model fitting problem (Elashoff et al., 2007a,b; Li et al., 2009, 2012; Andrinopoulou et al., 2014, 2015; Rajeswaran et al., 2018). When the number of longitudinal variables increases, it becomes increasingly difficult to use this strategy to maintain computational stability and avoid excessive computing time. Third, while there is previous literature on the prediction of future longitudinal biomarker trajectories (Taylor et al., 2005; Yu et al., 2008; Rizopoulos, 2012), this was done without conditioning on the fact that the future survival endpoint does not occur and hence is not suitable for our research problem (e.g., the predicted future GFR at year 3 is meaningless if the patient dies before that time).

In this paper, we propose a new type of joint model that avoids these limitations and is therefore suitable for the CKD research problem and beyond. It extends the basic idea of backward joint model (BJM) (Shen and Li, 2021) to the competing risk setting and also enables the prediction of future longitudinal renal biomarkers in the absence of death or ESRD. The model and estimation can be easily scaled for a large number of longitudinal variables because the dimension of the numerical integral is always capped at 1. For most model parameters, the log-likelihood has a concave shape, which facilitates convergence. The proposed method also comes with a simpler version that can be implemented quickly with standard statistical software to obtain consistent albeit slightly less efficient estimation. The proposed BJM is also flexible in the sense that it can use various competing risk models or longitudinal data models as its building blocks for the prediction.

2 Data, Estimands and Models

2.1 Data and notation

The training dataset has n subjects, indexed by $i = 1, 2, \dots, n$. Let \tilde{T}_i denote the true time to a terminal event and C_i denote the censoring time. All the time variables in this paper are expressed as the time gap since baseline unless stated otherwise. The terminal event can be one of J event types, denoted by $\tilde{D}_i \in \{1, 2, \dots, J\}$. In our motivating data application in CKD, $J = 2$, and the terminal event is either ESRD ($j = 1$) or death ($j = 2$). The observed survival time is $T_i = \min(\tilde{T}_i, C_i)$. The observed event type is $D_i = \delta_i \tilde{D}_i \in \{0, 1, \dots, J\}$, where the censoring indicator $\delta_i = \mathbf{1}(\tilde{T}_i < C_i)$ equals 1 when the terminal event is observed and 0 when censored. Let \mathbf{V}_i denote the vector of baseline covariates. Suppose that there are

M longitudinally measured continuous biomarkers, denoted by $m = 1, 2, \dots, M$. We denote the repeated measures of the m -th biomarker of subject i by \mathbf{Y}_{mi} , with the corresponding vector of time points \mathbf{t}_{mi} . The number of longitudinal biomarker measurements is n_{mi} , which varies by biomarker and subject. The measurement times of a biomarker may be irregularly spaced between baseline and T_i , and different biomarkers may be measured at different time points. Let $\mathbf{Y}_i = (\mathbf{Y}_{1i}^T, \mathbf{Y}_{2i}^T, \dots, \mathbf{Y}_{Mi}^T)^T$ and $\mathbf{t}_i = (\mathbf{t}_{1i}^T, \mathbf{t}_{2i}^T, \dots, \mathbf{t}_{Mi}^T)^T$ collect all the longitudinal biomarker data and their measurement times in vector forms. We follow two conventional assumptions from the joint modeling literature. First, the biomarker measurement times are non-informative in the sense that the distribution of \mathbf{t}_i in $(0, T_i)$ is independent of the rest of the data. Second, the censoring is independent in the sense that C_i is conditionally independent of \mathbf{Y}_i and \tilde{T}_i given \mathbf{V}_i .

2.2 Prediction estimands

The models in this paper are motivated by the research objective, estimating the predicted distribution of the survival and longitudinal outcomes given the longitudinal history prior to the time of prediction. Therefore, we must define the estimands of this prediction problem before describing the models. We use the subscript o to index a generic subject in the validation dataset. Let s be the time of prediction and $\overline{\mathbf{Y}_o(s)}$ represent the longitudinal biomarker history prior to s (i.e., all the biomarker measurements before s). Δ denotes a pre-specified prediction horizon. The prediction estimand of scientific interest is defined and derived in (1). This is the probability of having the terminal event of type j ($j = 1, 2, \dots, J$) in the next Δ years (or other time units), given that the subject is still at-risk at the prediction time s ($T_o > s$) and given the observed history $(\mathbf{V}_o, \overline{\mathbf{Y}_o(s)})$. The derivation used the independent censoring assumption.

$$P(s < \tilde{T}_o \leq s + \Delta, \tilde{D}_o = j | \overline{\mathbf{Y}_o(s)}, T_o > s, \mathbf{V}_o) = \frac{P(\overline{\mathbf{Y}_o(s)}, s < \tilde{T}_o \leq s + \Delta, \tilde{D}_o = j | \mathbf{V}_o)}{P(\overline{\mathbf{Y}_o(s)}, \tilde{T}_o > s | \mathbf{V}_o)}, \quad \forall j \quad (1)$$

We use $P(\cdot)$ to denote probability or probability density, when there is no ambiguity. We are also interested in the dynamic prediction of future longitudinal biomarker distribution. This is formulated as the estimand in (2) for a future time $t > s$. The notation $\mathbf{Y}_o(t)$ denotes the generic subject o 's longitudinal biomarker value at t .

$$P(\mathbf{Y}_o(t) = \mathbf{y} | \tilde{T}_o > t, \overline{\mathbf{Y}_o(s)}, T_o > s, \mathbf{V}_o) = \frac{P(\mathbf{Y}_o(t) = \mathbf{y}, \overline{\mathbf{Y}_o(s)}, \tilde{T}_o > t | \mathbf{V}_o)}{P(\overline{\mathbf{Y}_o(s)}, \tilde{T}_o > t | \mathbf{V}_o)}, \quad (2)$$

This is the probability density function of the longitudinal biomarker at a future time t , given that the subject is at-risk by the time of prediction ($T_o > s$), and the observed history $\{\overline{\mathbf{Y}_o(s)}, \mathbf{V}_o\}$, and conditional on the absence of the terminal event by time t . A key novel aspect of this definition is that the predicted longitudinal biomarker at a future time t can only be defined when the terminal event does not occur by that time. In our data application, for example, the GFR does not exist if the patient has reached ESRD or death. We may choose $t = s + \Delta$ to obtain the biomarker prediction at the horizon, or choose t to be any time between s and $s + \Delta$ to obtain the predicted longitudinal trajectory in $(s, s + \Delta)$. The notation in (2) is designed for the most general case that we predict the multivariate density of all the M biomarkers. In our data application, we are interested in

the single most important longitudinal biomarker and similar expression can be formulated for that situation. Given the estimated density function, various interpretable features of the density, such as quantiles, mean and mode, can be subsequently obtained, as illustrated in the data application.

2.3 Backward joint models with extrapolation or two parts

If the conditional joint distribution $P(\mathbf{Y}_o, \tilde{T}_o, \tilde{D}_o | \mathbf{V}_o)$ can be estimated from the training dataset, then the prediction estimands in (1) and (2) can be easily calculated. Since $P(\mathbf{Y}_o, \tilde{T}_o, \tilde{D}_o | \mathbf{V}_o) = P(\tilde{T}_o, \tilde{D}_o | \mathbf{V}_o)P(\mathbf{Y}_o | \tilde{T}_o, \tilde{D}_o, \mathbf{V}_o)$, we propose sub-models for the two conditionals. The first is a competing risk regression with baseline covariates. The second sub-model can be a multivariate linear mixed model when \mathbf{Y}_o is continuous. Since \mathbf{Y}_o occurs prior to \tilde{T}_o , we call this approach a “backward” joint model (BJM). This likelihood decomposition resembles the pattern mixture model in the missing data literature but there are fundamental differences in model formulation, estimation and scope of application, as elucidated previously (Shen and Li, 2021). From (1) and (2), all that is needed for prediction purposes is the conditional joint distribution $P(\mathbf{Y}_o, \tilde{T}_o, \tilde{D}_o | \mathbf{V}_o)$. In fact, any model that leads to the estimation of this joint distribution can be used here. The model does not have to reflect the data-generating mechanism in the sense that it consists of the conditional distributions of later data given earlier data. The data-generating mechanism of real data is usually far more complicated than a statistical model can describe.

Both prediction estimands involve $P(\overline{\mathbf{Y}_o(s)}, \tilde{T}_o > t | \mathbf{V}_o) = \int_t^\infty P(\overline{\mathbf{Y}_o(s)} | \tilde{T}_o = u, \mathbf{V}_o)P(\tilde{T}_o = u | \mathbf{V}_o)du$, ($t \geq s$). In typical biomedical studies, \tilde{T}_o and C_o have finite supports. We consider two study designs. First, there is a time τ_{max} such that $P(C_o > \tau_{max} | \mathbf{V}_o) > 0$ and $P(\tilde{T}_o \geq \tau_{max} | \mathbf{V}_o) = 0$, i.e., the support of C_o is longer than the support of \tilde{T}_o . Both $P(\overline{\mathbf{Y}_o(s)} | \tilde{T}_o = u, \mathbf{V}_o)$ and $P(\tilde{T}_o = u | \mathbf{V}_o)$ are identifiable at every u on the support of \tilde{T}_o , and we just need a sub-model for each conditional distribution. This is the design where the follow-up is generally longer than the survival time of study subjects. Second, there is a time τ_{max} such that $P(\tilde{T}_o > \tau_{max} | \mathbf{V}_o) > 0$ and $P(C_o > \tau_{max} | \mathbf{V}_o) = 0$ for at least some subjects in the population, i.e., the support of C_o is shorter than the support of \tilde{T}_o . $P(\overline{\mathbf{Y}_o(s)} | \tilde{T}_o = u, \mathbf{V}_o)$ and $P(\tilde{T}_o = u | \mathbf{V}_o)$ are not always identifiable from the data when $u > \tau_{max}$. This is the design where the follow-up is not long enough to estimate the entire survival function. To solve this problem, we write $P(\overline{\mathbf{Y}_o(s)}, \tilde{T}_o > t | \mathbf{V}_o)$ as

$$\int_t^{\tau_{max}} P(\overline{\mathbf{Y}_o(s)} | \tilde{T}_o = u, \mathbf{V}_o)P(\tilde{T}_o = u | \mathbf{V}_o)du + P(\overline{\mathbf{Y}_o(s)} | \tilde{T}_o > \tau_{max}, \mathbf{V}_o)P(\tilde{T}_o > \tau_{max} | \mathbf{V}_o). \quad (3)$$

A sub-model for survival data can identify both $P(\tilde{T}_o = u | \mathbf{V}_o)$, $t < u \leq \tau_{max}$, and $P(\tilde{T}_o > \tau_{max} | \mathbf{V}_o)$. Two sub-models for longitudinal data are needed to identify $P(\overline{\mathbf{Y}_o(s)} | \tilde{T}_o = u, \mathbf{V}_o)$, $t < u \leq \tau_{max}$ and $P(\overline{\mathbf{Y}_o(s)} | \tilde{T}_o > \tau_{max}, \mathbf{V}_o)$ for those with $\tilde{T} > \tau_{max}$. These subjects with $\tilde{T} > \tau_{max}$ are referred to as long-term survivors (LTS; Wang et al, 2020). In real data analysis, we can empirically use the estimated marginal distribution of \tilde{T} to decide whether the extra longitudinal sub-model for the LTS is needed. If the Kaplan-Meier curve of \tilde{T} descends to near 0, that suggests that the LTS group is likely very small. We call it the BJM with extrapolation (BJM-EX). The extrapolation means that the estimated distribution $P(\tilde{T} | \mathbf{V})$ extrapolates beyond the support of the data sample. Alternatively, the LTS sub-model is needed and we call it the two-part BJM (BJM-TP). For BJM-TP,

the prediction time $s < \tau_{max} - \Delta$ because there is no observed terminal event beyond τ_{max} and the model does not extrapolate beyond the data range. For BJM-EX, there is no such restriction because the model extrapolates.

2.4 Sub-models for competing risk outcomes

Any competing risk regression model with time-invariant covariates can be fitted to $\{T_i, D_i, \mathbf{V}_i; i = 1, 2, \dots, n\}$ and estimate $P(\tilde{T}_o, \tilde{D}_o | \mathbf{V}_o)$. Common choices include the cause-specific hazard models, the Fine-Gray sub-distribution hazard model, or the vertical modeling (Nicolaie et al., 2010), among others. We used vertical modeling in the numerical studies because it directly models $P(\tilde{T}_i | \mathbf{V}_i)$, which is convenient for predicting longitudinal data in (2). We compared the BJMs with vertical modeling and with cause-specific hazard models, and the predictive performances were similar in our data application.

The likelihood of a vertical model for $P(\tilde{T}_i, \tilde{D}_i | \mathbf{V}_i)$ can be factorized as the likelihood product of $P(\tilde{T}_i | \mathbf{V}_i)$ and $P(\tilde{D}_i | \tilde{T}_i, \mathbf{V}_i)$. The former can be formulated as a semi-parametric Cox model, a parametric Weibull model, or any other survival regression model that fits the data well. The latter is a multinomial regression model, according to Nicolaie et al.

(2010). Specifically, $P(\tilde{D}_i = j | \tilde{T}_i = t, \mathbf{V}_i) = \frac{\exp(\mathbf{B}(t)^T \boldsymbol{\xi}_j^{(\tilde{T})} + \mathbf{V}_i^T \boldsymbol{\xi}_j^{(\mathbf{V})})}{\sum_{j=1}^J \exp(\mathbf{B}(t)^T \boldsymbol{\xi}_j^{(\tilde{T})} + \mathbf{V}_i^T \boldsymbol{\xi}_j^{(\mathbf{V})})}$, $j = 1, \dots, J$.

The $\mathbf{B}(t)$ is a vector of pre-specified regression spline basis to accommodate the nonlinear effect of \tilde{T}_i on the event types. When there are two event types, this is a logistic regression with partially linear specification for the covariates \tilde{T}_i and \mathbf{V}_i . The estimation of vertical modeling follows Nicolaie et al. (2010).

2.5 Sub-models for longitudinal outcomes

For the BJM-EX, $P(\mathbf{Y}_o | \tilde{T}_o, \tilde{D}_o, \mathbf{V}_o)$ is modeled by a multivariate linear mixed model, with $T_i, D_i, \mathbf{V}_i, \mathbf{t}_i$ and their interactions as fixed-effect covariates and with random effects (intercept, or intercept and slope) to account for the longitudinal correlation and the correlation among different biomarkers. The sub-model of the m -th longitudinal biomarker ($m = 1, 2, \dots, M$) can be formulated in the following general form.

$$Y_{mi}(t) = \sum_{l=0}^L \vartheta_{ml}(\mathbf{V}_i, \phi(\tilde{T}_i), \tilde{D}_i) g_l(t) + \mathbf{u}_{mi}(t)^T \mathbf{b}_{mi} + \epsilon_{mi}(t) \quad , \quad t \in [0, \tilde{T}_i]. \quad (4)$$

$Y_{mi}(t)$ is subject i 's m -th biomarker, measured at time t . In the training data, $t \in \mathbf{t}_{mi}$. The first term describes the conditional mean trajectory (CMT), given baseline covariates (\mathbf{V}), terminal event time (\tilde{T}) and type (\tilde{D}). The CMT is defined for subjects with the same trajectory lengths (\tilde{T}), because it does not lead to proper interpretation to average the longitudinal biomarker trajectories of different lengths when the follow-up duration is correlated with longitudinal data, a defining feature of joint modeling problems that is sometimes called informative dropout. The second term includes random effects that describe the subject-specific, mean-zero deviation from the CMT. The random intercept ($\mathbf{u}_{mi}(t) = 1$), random intercept plus slope ($\mathbf{u}_{mi}(t) = (1, t)^T$), or other nonlinear random effect terms can be used. The $g_l(t), l = 0, 1, \dots, L$ are basis functions that characterize the shape of the CMT. For example, the linear CMT has $L = 1$, $g_0(t) = 1$, and $g_1(t) = t$.

The coefficients of the basis functions, $\vartheta_{ml}(\mathbf{V}_i, g_1(\tilde{T}_i), \tilde{D}_i)$, are interpreted as the intercept, slope, etc., allowing the CMT to vary with \mathbf{V}_i , \tilde{T}_i and \tilde{D}_i . For example, $\vartheta_{m0}(\mathbf{V}_i, \phi(\tilde{T}_i), \tilde{D}_i) = \boldsymbol{\beta}_{m1}^T \mathbf{V}_i + \nu_{m0} \tilde{D}_i + \nu_{m2} \phi(\tilde{T}_i) + \nu_{m4} \phi(\tilde{T}_i) \tilde{D}_i$, $\vartheta_{m1}(\mathbf{V}_i, \tilde{T}_i, \tilde{D}_i) = \boldsymbol{\beta}_{m2}^T \mathbf{V}_i + \nu_{m1} \tilde{D}_i + \nu_{m3} \phi(\tilde{T}_i) + \nu_{m5} \phi(\tilde{T}_i) \tilde{D}_i$. The pre-specified transformation $\phi(\cdot)$, e.g. log, may be used to reduce the skewness of the time variable \tilde{T}_i .

The residuals $\varepsilon_{mi}(t)$ are independent noises with mean zero and variance $\sigma_{e,m}^2$. Extensions to residuals with auto-correlation are straightforward. The random effects from all M biomarkers $\mathbf{b}_i = (\mathbf{b}_{1i}^T, \mathbf{b}_{2i}^T, \dots, \mathbf{b}_{Mi}^T)^T$ follows a multivariate normal distribution with mean zero and covariance matrix $\boldsymbol{\Omega}$. When model (4) has random intercept and slope, $\boldsymbol{\Omega}$ is a $2M \times 2M$ matrix that is not restricted to be block diagonal, allowing the biomarkers to be correlated.

The BJM-TP has an extra longitudinal sub-model for the LTS:

$$Y_{mi}(t) = \sum_{l=0}^L \vartheta_{ml}^e(\mathbf{V}_i) g_l(t) + \mathbf{u}_{mi}^e(t)^T \mathbf{b}_{mi}^e + \varepsilon_{mi}^e(t) \quad , \quad t \in [0, \tau_{max}) \text{ and } \tilde{T}_i > \tau_{max}. \quad (5)$$

The superscript e symbolizes quantities in the ‘‘extra’’ LTS model. The model formulation and interpretation are similar to (4) but with a few differences. First, model (5) does not involve \tilde{T}_i and \tilde{D}_i in the covariates because the LTS includes all subjects who survive beyond τ_{max} regardless of their actual \tilde{T}_i and \tilde{D}_i . Second, since the LTS is a heterogeneous group, models (5) and (4) cannot have the same random effect variance or residual variance. Presumably, the variances are larger in model (5).

3 Estimation

The BJM’s likelihood factorization $P(\mathbf{Y}_o, \tilde{T}_o, \tilde{D}_o | \mathbf{V}_o) = P(\tilde{T}_o, \tilde{D}_o | \mathbf{V}_o) P(\mathbf{Y}_o | \tilde{T}_o, \tilde{D}_o, \mathbf{V}_o)$ suggests a two-step estimation procedure. In the first step, we fit the competing risk regression model (Section 2.4). Many standard software packages are available. In the second step, we estimate $P(\mathbf{Y}_o | \tilde{T}_o, \tilde{D}_o, \mathbf{V}_o)$ from the longitudinal sub-models in Section 2.5 and this is the focus of this section. We propose two approaches. Section 3.1 presents a simple method that can be conveniently implemented with standard linear mixed model software. This method only uses training data subjects whose terminal event times are observed and those still at-risk by τ_{max} . Since many censored data are not used, we call this approach the complete-case analysis (CCA). A remarkably useful feature of the BJM is that the CCA produces consistent estimation, albeit less efficient. In contrast, typical joint models of longitudinal and survival data would require specialized software and they have limited functionality and flexibility. The CCA of BJM enables quick and convenient exploratory analysis, model building, model assumption diagnosis, and preliminary prediction accuracy assessment. Once the model specification is completed, we can use the fully likelihood-based analysis in Section 3.2 to obtain efficient estimators and the final results of the prediction model and prediction accuracy.

3.1 Complete-case analysis (CCA)

To see why the parameters of longitudinal sub-model can be consistently estimated with the complete cases in the training data (i.e., $D_i \neq 0$), we observe that, for any $j = 1, 2, \dots, J$,

$P(\mathbf{Y}|\tilde{T} = t, \tilde{D} = j, \mathbf{V}) = P(\mathbf{Y}|\tilde{T} = t, C > t, \tilde{D} = j, \mathbf{V}) = P(\mathbf{Y}|T = t, D = j, \mathbf{V})$. The simple derivation is justified by the conditional independence of censoring. It holds at any $t \in (0, \infty)$ for the BJM-EX, and any $t \in (0, \tau_{max})$ for the BJM-TP. $P(\mathbf{Y}|T = t, D = j, \mathbf{V})$ can be estimated via a linear mixed model according to the specification in (4). Additionally, $P(\mathbf{Y}|\tilde{T} > \tau_{max}, \mathbf{V}) = P(\mathbf{Y}|\tilde{T} > \tau_{max}, C > \tau_{max}, \mathbf{V}) = P(\mathbf{Y}|T > \tau_{max}, \mathbf{V})$ in the BJM-TP. Hence, model (5) can be estimated from the subset of training data with $T_i > \tau_{max}$. Consistent estimation of CCA has been demonstrated in previous research on models with a similar likelihood factorization (Li et al., 2018; Wang et al., 2020; Shen and Li, 2021; Wang et al., 2023).

3.2 EM algorithm for the analysis of all data

This section describes the EM algorithm that calculates the maximum likelihood estimators (MLE) of the parameters in the longitudinal sub-models. Since it uses both censored and non-censored data, the estimation is more efficient than the CCA (Li et al., 2018; Wang et al., 2020; Shen and Li, 2021). The censored \tilde{T}_i and \tilde{D}_i are treated as missing data in the complete data log-likelihood. Since the parameters in the competing risk sub-model are estimated consistently in Section 2.4 and are fixed at their estimated values during the EM iterations, the method in this section is a type of pseudo maximum likelihood estimation (Gong and Samaniego, 1981).

Let Θ denote the parameters of the longitudinal sub-model. With BJM-TP, Θ includes additionally the parameters Θ^e from the LTS sub-model (5). The estimated parameters from the survival sub-model are denoted by $\hat{\Theta}_{surv}$. Since $\hat{\Theta}_{surv}$ is fixed throughout the EM iterations, we omit it for the formula below. In the following, we mainly describe the EM algorithm of the BJM-EX, but will point out the changes needed when the BJM-TP is used. The complete data log-likelihood is $\sum_{i=1}^n \left\{ \log P(\mathbf{Y}_i|\tilde{T}_i, \tilde{D}_i, \mathbf{V}_i; \Theta) + \log P(\tilde{T}_i, \tilde{D}_i|\mathbf{V}_i) \right\}$. The observed data of all subjects in the training dataset is collected in $\{\mathbf{Y}, \mathbf{T}, \boldsymbol{\delta}, \mathbf{D}, \mathbf{V}\}$. The EM algorithm uses the consistent estimators from the CCA as the initial values in the first EM iteration. At the beginning of the q -th iteration ($q = 1, 2, \dots$), the estimated parameter is denoted by $\hat{\Theta}^{(q)}$.

In the E-step of the q -th iteration, we calculate the conditional expectation of the complete data log-likelihood as in (6). This expectation is taken over the conditional distribution of the missing data (censored \tilde{T}_i and \tilde{D}_i) given the observed data, with parameters in this distribution set at $\hat{\Theta}^{(q)}$.

$$\begin{aligned} & \sum_{i=1}^n E_{(\tilde{T}_i, \tilde{D}_i)} \left\{ \log P(\mathbf{Y}_i|\tilde{T}_i, \tilde{D}_i, \mathbf{V}_i; \Theta^{(q+1)}) + \log P(\tilde{T}_i, \tilde{D}_i|\mathbf{V}_i) \middle| \mathbf{Y}, \mathbf{T}, \boldsymbol{\delta}, \mathbf{D}; \hat{\Theta}^{(q)} \right\} \\ & \propto \sum_{i=1}^n \sum_{j=1}^J \int_{\tilde{T}_i=T_i}^{\infty} \left\{ \log P(\mathbf{Y}_i|\tilde{T}_i, \tilde{D}_i = j, \mathbf{V}_i; \Theta^{(q+1)}) \right\} P(\tilde{T}_i, \tilde{D}_i = j|\mathbf{Y}, \mathbf{T}, \boldsymbol{\delta}, \mathbf{D}; \hat{\Theta}^{(q)}) d\tilde{T}_i \end{aligned} \quad (6)$$

There is always a one-dimensional integral in (6), regardless of how many longitudinal biomarker variables are involved. This integral is needed only for censored subjects. In contrast, the widely used shared random effects joint model (Rizopoulos, 2012) has n integrals in its likelihood, and the dimension of the integral increases with the number of longitudinal variables. This feature is the key reason that BJM is computationally much

easier. The integration in (6) goes from T_i to ∞ . With BJM-TP, this calculation is split into two parts, analogously to (3). The first integrates from T_i to τ_{max} using model (4) and the second uses the LTS model (5).

The integral in (6) can be calculated with the trapezoidal rule. If T_i is a censoring time, we assume that \tilde{T}_i falls in one of a series of pre-specified connected intervals, denoted by $\{\mathbb{L}_{ik} = [a_{ik}, b_{ik}); k = 1, \dots, K_i\}$. The intervals are connected (e.g., $b_{ik} = a_{i(k+1)}$) and starts from T_i ($a_{i1} = T_i$). With BJM-EX, we can set the ending time of the last interval at a very large survival time (e.g., 100 year old). With BJM-TP, the last interval is $[\tau_{max}, \infty)$ and the LTS model is used on this interval. A moderate K_i can produce accurate results when the residual survival beyond T_i is not very large or when the integrand is not excessively wiggly (Li et al., 2018). The target function (6) of BJM-EX then becomes:

$$\sum_{i=1}^n \sum_{k=1}^{K_i} \sum_{j=1}^J \left\{ \log P(\mathbf{Y}_i | \tilde{T}_i = \frac{a_{ik} + b_{ik}}{2}, \tilde{D}_i = j, \mathbf{V}_i; \Theta^{(q+1)}) \right\} P(\tilde{T}_i \in \mathbb{L}_{ik}, \tilde{D}_i = j | \mathbf{Y}, \mathbf{T}, \boldsymbol{\delta}, \mathbf{D}; \hat{\Theta}^{(q)}). \quad (7)$$

With BJM-TP, the target function is the same except that the terms corresponding to the last interval (\mathbb{L}_{iK_i}) are replaced by $\left\{ \log P(\mathbf{Y}_i | \tilde{T}_i \in \mathbb{L}_{iK_i}, \mathbf{V}_i; \Theta^{(q+1)}) \right\} P(\tilde{T}_i \in \mathbb{L}_{iK_i} | \mathbf{Y}, \mathbf{T}, \boldsymbol{\delta}, \mathbf{D}; \hat{\Theta}^{(q)})$.

In the M-step, (7) is maximized with respect to $\Theta^{(q+1)}$, producing an updated estimator $\hat{\Theta}^{(q+1)}$ that will enter the next ($q+1$ -th) iteration. The only terms containing the unknown parameters are $\log P(\mathbf{Y}_i | \tilde{T}_i = (a_{ik} + b_{ik})/2, \tilde{D}_i = j, \mathbf{V}_i; \Theta^{(q+1)})$. These are log of multivariate normal density functions, which are quadratic forms of the regression coefficients in the longitudinal sub-models. $P(\tilde{T}_i \in \mathbb{L}_{ik}, \tilde{D}_i = j | \mathbf{Y}, \mathbf{T}, \boldsymbol{\delta}, \mathbf{D}; \hat{\Theta}^{(q)})$ is calculated in the E-step and treated as fixed in the maximization of the M-step. Therefore, the regression coefficients have closed-form solutions (the variance-covariance matrices of the random effects do not; see below). This feature, in conjunction with using the consistent estimators from the CCA as the initial value of the EM algorithm, speeds up the computation considerably and improves the robustness of the iterations. We have observed a 100% convergence rate with the EM and the computing time is much shorter compared to the shared random effects joint model.

The number of regression coefficients in the BJM increases linearly with the number of longitudinal biomarkers. However, the number of parameters in the variance-covariance matrix of the random effects goes up quadratically, which poses a challenge for any joint models that aim to accommodate multivariate longitudinal data. However, the BJM has a special feature that helps avoid this computational burden. During the EM algorithm, we fix the variance-covariance matrix of the random effects and residuals at their consistently estimated values from the CCA. This approach is justified by the pseudo maximum likelihood estimation (Gong and Samaniego, 1981).

3.3 Variance estimation

We use the bootstrap for variance estimation. Specifically, we randomly sample the subjects in the training data with replacement, creating a bootstrap dataset. The bootstrap dataset is put through the BJM estimation procedure to produce point estimators of the model parameters. This process is repeated 200 times, and the variances of the estimated model parameters can be calculated as the sample variance of the 200 point estimators. For a

subject in the validation dataset, the prediction (1) or (2) is a function of the estimated BJM model parameters and the subject’s data prior to the prediction time. The variance of the prediction can be calculated by Delta-method to account for the sampling variability of the estimated BJM model. As an alternative approach that avoids the mathematical derivation of the Delta-method, we can also calculate the prediction using each of the 200 estimated model parameters from the bootstrap. The resulting sample variance quantifies the variance of the prediction. Since the estimated model parameters are approximately normal, a Wald-type confidence interval can be obtained from the estimated variance.

3.4 Prediction accuracy measures

We follow the previous literature in choosing the prediction accuracy measures. For predicting competing risk outcomes, we use the time-dependent Brier score (BS) and the time-dependent AUC (Definition A in Wu and Li, 2018), both designed for competing risk data. For predicting the future longitudinal biomarkers, we use RMSE (root mean squared error). Since our data application is CKD research, we also use two commonly used measures in that field for predicting GFR, the P30 and P50 (Levey, 1999). They are the proportions of subjects for whom the predicted GFR falls within 30% or 50% of the observed GFR at the horizon. Higher AUC, lower BS, lower RMSE, higher P30 and P50 suggest better predictive accuracy. When the GFR measurements are irregularly spaced and there is no GFR data at the horizon, the closest measurement prior to the horizon is used.

4 Data Application

We illustrate the proposed BJM methodology by analyzing data from the African American Study of Kidney Disease and Hypertension (AASK) Cohort Study. AASK is a longitudinal cohort study of 1,094 CKD subjects. Detailed descriptions of AASK data were reported previously (Li et al., 2016; Wu et al., 2020). By the end of the follow-up, 318 subjects (29%) reached ESRD and 176 subjects (16%) died before reaching ESRD. We did not consider survival after ESRD in a semi-competing risk analysis because the patient experience and treatments were substantially different after reaching ESRD. We used two baseline predictors, age and gender. We considered three longitudinally measured predictive biomarkers, the estimated glomerular filtration rate (eGFR) using the MDRD equation, 24-hour urine protein to creatinine ratio (UPCr), and serum albumin. These biomarkers have known clinical relationships with the survival outcomes and hence are ideal choices as predictors.

Web Figure S1 displays the Kaplan-Meier curve of the composite endpoint of ESRD or death, whichever occurs first, and the cumulative incidence functions of ESRD and death separately. The distribution of the composite event in this population can be estimated up to 12 years, with more than 40% of the events expected beyond that time. This supported the use of BJM-TP. For comparison purposes, we also presented results from BJM-EX. We set $\tau_{max} = 12$ years, the maximum observed event time in the data. We experimented with both vertical modeling and cause-specific hazard modeling as the survival sub-model, and they produced similar prediction accuracy. The reported results here came from BJM with vertical modeling. Figure 3 displays the CMTs of eGFR, which are approximately linear

and suggest a clear association with the time of the composite endpoint and event types, with an interaction between the two.

Including more predictive longitudinal biomarkers improves the prediction accuracy. The BJM remains computationally convenient in this situation. To illustrate the benefit of using more longitudinal predictors, we considered BJMs with one (BJM-1, with eGFR), two (BJM-2, with eGFR and UPCr), or three (BJM-3, with eGFR, UPCr, and albumin) longitudinal biomarkers. Our EM algorithm achieved 100% convergence rates in these analyses. Since this paper is mainly about prediction, we focus on prediction results here, and defer the extensive details on model specification, parameter estimation and interpretation, and sensitivity analysis to the Web Appendix. With BJM-3, the extrapolation model (EX) has 48 parameters and the two-part model (TP) has 72 parameters. The BJM includes a competing risk regression model and a linear mixed model for each longitudinal parameter. These are conventional statistical models in which all the parameters are well identified. The number of parameters characterizing the correlation of multiple longitudinal biomarkers increases quadratically with the number of biomarkers, but these parameters are inevitable in any joint models with multivariate longitudinal biomarkers. The TP model has 50% more parameters because it uses two parts to improve flexibility without extrapolation, but all the parameters in its LTS sub-model are identified.

We used five-fold cross-validation to evaluate the prediction accuracy at a horizon of 3 years (Table 1). Additional results under 1-year horizon are reported in the Web Appendix. In predicting ESRD and death, Table 1 shows that BJMs with more longitudinal biomarkers generally performed better than those with less, with BJM-3-TP performing similarly to or better than all other methods in both AUC and BS. The TP methods generally performed better than the EX methods, likely because it is less prone to model misspecification when the tail distribution of the composite event cannot be estimated. The performance of BJM-3-EX rose on par with their counterpart TP model (BJM-3-TP), while BJM-2-EX and BJM-1-EX did not. The performance of EX models is more difficult to speculate about probably because the accuracy of the extrapolation is unknown and cannot be verified from data. Nonetheless, BJM-3-EX achieved similar predictive accuracy for ESRD and death as BJM-3-TP did but with fewer parameters, making it an empirically useful model for prediction purposes. In predicting the eGFR, TP methods substantially outperformed EX methods. The BS appears to be more sensitive to between-method differences than the AUC, possibly because the latter is rank-based. The incidence of ESRD can be predicted with very high AUC because the treatment decision of dialysis or renal transplantation is strongly influenced by the patient’s eGFR.

For comparison purposes, we fitted the widely-used shared random effects joint model (SJM) using the `JMbayes2` package in R. The model included all three longitudinal biomarkers (i.e., denoted by SJM-3 in Table 1), whose trajectories were modeled by linear mixed models with subject-specific random intercepts and random slopes, and these random effects were shared with the cause-specific hazard models as covariates. The BJMs outperformed the SJM in predicting ESRD and death. The results of eGFR prediction are mixed. However, it seems that the SJM does not condition on the absence of the composite event when predicting eGFR (Section 7.2 of Rizopoulos, 2012), which makes this comparison difficult. The BJM is computationally much faster than the SJM. To complete the five-fold cross-validation on a personal computer with 2.9 GHz CPU and 32 GB RAM, SJM-3 took 3 hours whereas BJM-3-TP with EM algorithm took 13 minutes. The CCA of BJM can

implemented with standard statistical software and the computing time is almost negligible.

Figure 4 depicts individual dynamic predictions of ESRD and death for two AASK patients. The patient on the left (A) had stable eGFR before year 3 but went into a steady decline from year 3 to year 8. The UPCr also increased over time, indicating increasing kidney damage. The predicted future probability of ESRD increases sharply in response. This patient eventually reached ESRD. The patient on the right had stable biomarkers and the predicted ESRD risk is low. The mortality risk, however, increases over time, presumably due to both aging and low ESRD risk (a competing risk phenomenon). Figure 5 illustrates two useful graphical presentations of the joint prediction of competing risk and longitudinal outcomes. The first uses the quantile curves to visualize how the predicted eGFR distribution conditional on absence of ESRD or death varies over time, in addition to the predicted cumulative incidence functions of ESRD and death. This patient’s eGFR was within a stable range between the two prediction times, and the predicted ESRD was similar as a result. However, we can observe a subtle decrease in the predicted eGFR in the second prediction, perhaps due to the lower observed eGFR just prior to the prediction and increased UPCr. The cumulative incidence of death increases due to time elapsing and aging. The second graphical presentation is clinically more interpretable (Hu et al., 2012), where the future probabilities of being in each CKD stage and death are visualized. From year 2 to year 4, the eGFR stabilized around 30, which triggered the model to lower the probability of ESRD but enlarge the probability area corresponding to CKD stage 4 (eGFR between 15 and 29). The probability of death increased slightly due to time elapsing and aging.

We performed a sensitivity analysis to study whether the prediction accuracy is affected by the specifications for random effects in (4), random intercept only or both random intercept and slope, and the choices of $\phi(\cdot)$ in that model, $\phi(t) = \log(t)$ or $\phi(t) = t$. The random slope adds flexibility to the individual-level longitudinal trajectories within each survival stratum (i.e., given \tilde{T}) but also adds more parameters to the variance matrix for the random effects. A log transformation may fit the data better when \tilde{T} is skewed. Web Table S4 shows that the prediction accuracy is not sensitive to these alternative formulations. We speculate that the survival time in the AASK data is not very skewed (Web Figure S1). For this reason, we used the simpler model specification of random intercept and no log transformation.

5 Simulation

We conducted simulations to study the finite sample performance of the proposed estimation procedure for both TP and EX models, and to compare the relative efficiency of CCA vs. EM algorithm. The CCA and EM methods both produce consistent estimation, but CCA is easier to use, making it worthwhile to assess its efficiency cost. We already compared the predictive performance of BJM and SJM in the AASK data. We do not compare them in the simulations because they operate under different modeling assumptions and it is impossible to simulate data so that both are correctly specified. Within the likelihood framework, consistent and efficient estimation of the BJM guarantees optimal predictive accuracy.

We conducted and reported simulation studies for the BJM-EX and BJM-TP separately.

In each study, we simulated 300 independent Monte Carlo datasets of n subjects from the BJM-EX model (or BJM-TP model), $n = 300$ or $1,000$, analyzed each dataset using both the CCA and EM algorithm, and calculated the bias of estimated model parameters and the relative efficiency between CCA and EM. We simulated one baseline covariate and three longitudinal biomarkers. The longitudinal sub-models had a linear CMT and random intercept. The competing risk model is a vertical model with a Weibull regression for the time to composite event. The censoring rate is 40% in the BJM-EX data. For BJM-TP, the overall censoring rate is 40% and 20% subjects were censored at τ_{max} . The BJM-EX and BJM-TP were fit to their respective datasets so that we can evaluate the estimation methods under the correct model specification. The CCA was used to obtain the initial values for the EM. All EM algorithms converged under the criterion that all longitudinal sub-model parameters differed by no more than 10^{-4} in consecutive iterations. Further details of the data-generating schemes are in the Web Appendix. Figure 1 shows that the finite-sample biases of the EM estimators are generally small and drop to nearly zero when the sample size increases from 300 to 1,000, supporting consistent estimation. The EM algorithm has notable efficiency improvement over the CCA, especially among the LTS sub-model parameters, probably because the CCA only uses the subjects at-risk by τ_{max} to estimate the LTS, which could have a small sample size.

6 Discussion

While the idea of backward joint modeling has been proposed for dynamic prediction (Shen and Li, 2021) and non-dynamic prediction (Li et al., 2018) problems, this paper is novel in several aspects: predicting competing risk outcomes, predicting the future distribution of longitudinal outcome conditional on being at risk, dual approaches (EX and TP) designed for different scenarios. The estimation algorithm of BJM ensures that model fitting remains computationally tractable with a large number of longitudinal variables. This is a common issue in prediction problems, but there is currently no research on joint modeling that guarantees computationally feasible algorithms. We compared the prediction accuracy of BJM and the widely used SJM in our data application, and BJM performed notably better. While a generalizable conclusion cannot usually be drawn from one data analysis, and it is difficult to compare the prediction accuracy in simulations because BJM and SJM operate under different modeling assumptions, there are two features in the BJM that help improve its predictive performance. The first is model formulation. The SJM was proposed decades ago for explaining the association between longitudinal and survival data, or for informative dropout problems. It was recently repurposed for use in dynamic prediction problems (Rizopoulos, 2011). In contrast, the BJM was designed from the ground up for dynamic prediction. As shown in Section 2, we first proposed the predictive estimand in (1) and (2) and then proposed a sub-model for each component in that estimand. Any appropriate sub-models for those components can be used in combination to improve prediction accuracy in various contexts, an interesting topic for future research. The second is model estimation. The SJM must be estimated by specialized software, which often offers limited flexibility. The lengthy computing time may also limit the scope of exploration. The BJM is much faster to estimate, and the model formulation can even be explored in CCA with standard software. We believe that the ease of estimation accelerates the development of BJM

variants for various research problems.

Another approach for dynamic prediction is the landmark modeling (van Houwelingen and Putter, 2011; Zheng and Heagerty, 2005). The joint modeling has many advantages over landmark modeling, including efficient likelihood-based estimation and easily incorporating the longitudinal history into the prediction. However, the landmark modeling is easy to implement, often with standard software, and it can handle large number of predictor variables (Li et al., 2023). With BJM, we have made joint modeling as computationally efficient, scalable, and easy to develop as landmark modeling. In addition, we are not aware of any landmark modeling approach that can predict future longitudinal data distribution. It is not straightforward with landmark modeling because the prediction of longitudinal data must be made conditional on the absence of a future clinical event, which requires modeling their joint distribution.

A limitation of this paper is that the longitudinal sub-models are parametric. The BJM models the CMT, not the individual-level trajectories. The CMT usually has less curvature and hence a parametric model may suffice. Model checking can also be done conveniently using CCA. Nonetheless, it is difficult to ensure that many longitudinal biomarkers are all modeled adequately with parametric models. Future work is needed to improve the flexibility of the fixed effect part with semi-parametric or non-parametric specification. The random effect part can also be improved by using penalized splines for subject-specific trajectory deviation from the CMT, though that would cause a substantial increase in the number of parameters in the covariance matrix of spline coefficients. However, this difficulty challenges all joint models with multivariate nonlinear longitudinal trajectories. Recent work suggested that, even if the random effect part is misspecified, the rest of the BJM model can be estimated consistently (Wang et al., 2023). In the sensitivity analysis (Web Table S4), we found that adding a random slope causes little change in the prediction accuracy. Since the BJM characterizes the association between survival outcome and longitudinal biomarkers through the fixed effects (as opposed to using random effects, such as in the SJM; Shen and Li, 2021), it remains to be studied whether the BJM is robust to misspecification of the random effect part. Another limitation of the BJM is that it sometimes requires an extra LTS sub-model. SJM does not have this need because it uses a time-varying hazard function. While the LTS can be easily estimated, it increases the number of parameters by about 50%. At a chosen τ_{max} , the percent of subjects contributing to the LTS estimation is $P(\tilde{T} > \tau_{max})P(C > \tau_{max})$. The censoring distribution may depend on staggered study entry, administrative censoring, and dropout patterns. When $P(C > \tau_{max})$ is low, we may need to decrease τ_{max} to ensure enough sample size for the LTS estimation. The longitudinal and survival data beyond τ_{max} are artificially censored as a result.

Acknowledgements

This research is supported in part by NIH grants P30CA016672 and R01DK118079.

Supporting Information

Web Appendices, Tables, and Figures are available with this paper.

References

- Andrinopoulou, E.-R., Harhay, M. O., Ratcliffe, S. J., and Rizopoulos, D. (2021). Reflection on modern methods: Dynamic prediction using joint models of longitudinal and time-to-event data. *International Journal of Epidemiology* **50**, 1731–1743.
- Andrinopoulou, E.-R., Rizopoulos, D., Takkenberg, J. J., and Lesaffre, E. (2015). Combined dynamic predictions using joint models of two longitudinal outcomes and competing risk data. *Statistical Methods in Medical Research* **26**, 1787–1801.
- Andrinopoulou, E.-R., Rizopoulos, D., Takkenberg, J. J. M., and Lesaffre, E. (2014). Joint modeling of two longitudinal outcomes and competing risk data. *Statistics in Medicine* **33**, 3167–3178.
- Appel, L. J., Grams, M., Woodward, M., Harris, K., Arima, H., Chalmers, J., Yatsuya, H., Tamakoshi, K., Li, Y., Coresh, J., et al. (2023). Estimated glomerular filtration rate, albuminuria, and adverse outcomes: An individual-participant data meta-analysis. *JAMA* **330**, 1266–1277.
- Elashoff, R., Li, G., and Li, N. (2016). *Joint Modeling of Longitudinal and Time-to-Event Data*. Chapman and Hall/CRC.
- Elashoff, R. M., Li, G., and Li, N. (2007a). An approach to joint analysis of longitudinal measurements and competing risks failure time data. *Statistics in Medicine* **26**, 2813–2835.
- Elashoff, R. M., Li, G., and Li, N. (2007b). A joint model for longitudinal measurements and survival data in the presence of multiple failure types. *Biometrics* **64**, 762–771.
- Gong, G. and Samaniego, F. J. (1981). Pseudo maximum likelihood estimation: Theory and applications. *The Annals of Statistics* **9**, 861–869.
- Hu, B., Li, L., Wang, X., and Greene, T. (2012). Nonparametric multistate representations of survival and longitudinal data with measurement error. *Statistics in Medicine* **31**, 2303–2317.
- Levey, A. S. (1999). A more accurate method to estimate glomerular filtration rate from serum creatinine: A new prediction equation. *Annals of Internal Medicine* **130**, 461.
- Li, L., Luo, S., Hu, B., and Greene, T. (2016). Dynamic prediction of renal failure using longitudinal biomarkers in a cohort study of chronic kidney disease. *Statistics in Biosciences* **9**, 357–378.
- Li, L., Wu, C.-H., Ning, J., Huang, X., Shih, Y.-C. T., and Shen, Y. (2018). Semiparametric estimation of longitudinal medical cost trajectory. *Journal of the American Statistical Association* **113**, 582–592.
- Li, N., Elashoff, R. M., Li, G., and Saver, J. (2009). Joint modeling of longitudinal ordinal data and competing risks survival times and analysis of the NINDS rt-PA stroke trial. *Statistics in Medicine* **29**, 546–557.

- Li, N., Elashoff, R. M., Li, G., and Tseng, C. (2012). Joint analysis of bivariate longitudinal ordinal outcomes and competing risks survival times with nonparametric distributions for random effects. *Statistics in Medicine* **31**, 1707–1721.
- Li, W., Li, L., and Astor, B. C. (2023). A comparison of two approaches to dynamic prediction: Joint modeling and landmark modeling. *Statistics in Medicine* **42**, 2101–2115.
- Lim, D. K. E., Boyd, J. H., Thomas, E., Chakera, A., Tippaya, S., Irish, A., Manuel, J., Betts, K., and Robinson, S. (2022). Prediction models used in the progression of chronic kidney disease: A scoping review. *PLOS ONE* **17**, e0271619.
- Nicolaie, M. A., van Houwelingen, H. C., and Putter, H. (2010). Vertical modeling: A pattern mixture approach for competing risks modeling. *Statistics in Medicine* **29**, 1190–1205.
- Rajeswaran, J., Blackstone, E. H., and Barnard, J. (2018). Joint modeling of multivariate longitudinal data and competing risks using multiphase sub-models. *Statistics in Biosciences* **10**, 651–685.
- Rizopoulos, D. (2011). Dynamic predictions and prospective accuracy in joint models for longitudinal and time-to-event data. *Biometrics* **67**, 819–829.
- Rizopoulos, D. (2012). *Joint Models for Longitudinal and Time-to-Event Data*. Chapman and Hall/CRC.
- Shen, F. and Li, L. (2021). Backward joint model and dynamic prediction of survival with multivariate longitudinal data. *Statistics in Medicine* **40**, 4395–4409.
- Taylor, J. M., Yu, M., and Sandler, H. M. (2005). Individualized predictions of disease progression following radiation therapy for prostate cancer. *Journal of Clinical Oncology* **23**, 816–825.
- van Houwelingen, H. and Putter, H. (2011). *Dynamic Prediction in Clinical Survival Analysis*. CRC Press.
- Wang, S., Ning, J., Xu, Y., Shih, T. Y., Shen, Y., and Li, L. (2023). Statistical modeling of longitudinal medical cost trajectory with insurance claims data. *Annals of Applied Statistics* page In press.
- Wang, S., Shen, Y., Shih, Y.-C. T., Xu, Y., and Li, L. (2020). Statistical modeling of longitudinal medical cost trajectory: renal cell cancer care cost analyses. *Biostatistics* **24**, 244–261.
- Wang, Y., Nan, B., and Kalbfleisch, J. D. (2023). Kernel estimation of bivariate time-varying coefficient model for longitudinal data with terminal event. *Journal of the American Statistical Association* pages 1–10.
- Wu, C. and Li, L. (2018). Quantifying and estimating the predictive accuracy for censored time-to-event data with competing risks. *Statistics in Medicine* **37**, 3106–3124.

- Wu, C., Li, L., and Li, R. (2020). Dynamic prediction of competing risk events using landmark sub-distribution hazard model with multiple longitudinal biomarkers. *Statistical Methods in Medical Research* **29**, 3179–3191.
- Yu, M., Taylor, J. M. G., and Sandler, H. M. (2008). Individual prediction in prostate cancer studies using a joint longitudinal survival–cure model. *Journal of the American Statistical Association* **103**, 178–187.
- Zheng, Y. and Heagerty, P. J. (2005). Partly conditional survival models for longitudinal data. *Biometrics* **61**, 379–391.

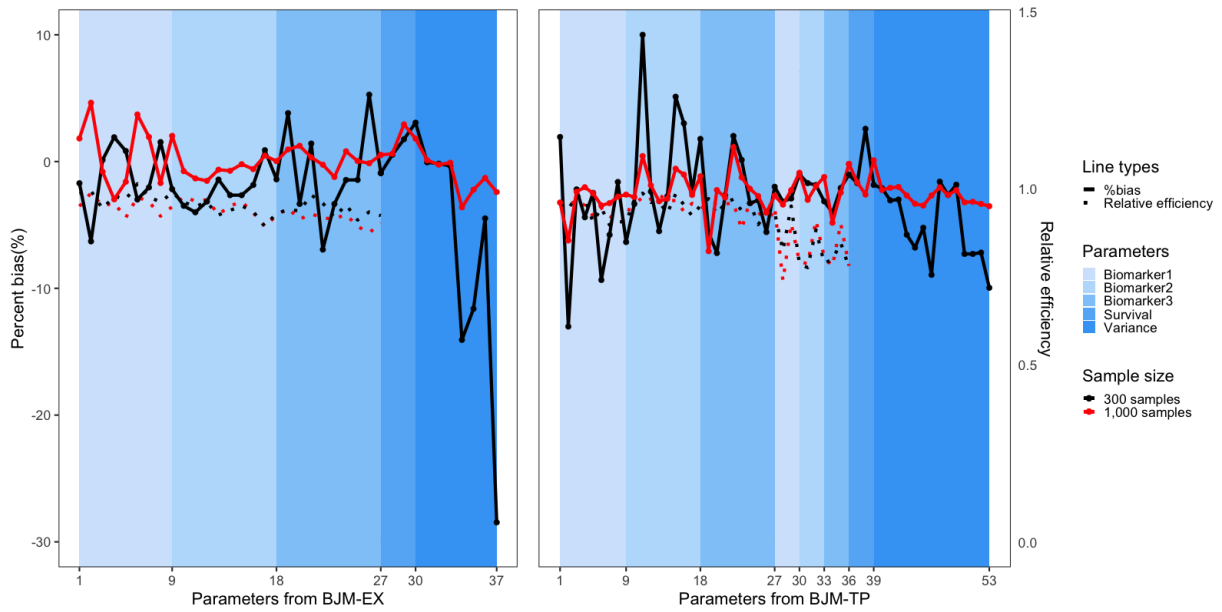


Figure 1: *Bias and efficiency of the BJM estimation in simulations (left: BJM-3-EX; right: BJM-3-TP). The horizontal axis is the index of parameters, grouped by their roles in the model. For better visualization, we used different background colors for different groups of parameters. For the EX model, the parameter groups from left to the right are longitudinal sub-models for biomarkers 1-3, survival sub-model, and variance-covariance matrix. For the TP model, the parameter groups from left to the right are longitudinal sub-models for biomarkers 1-3, longitudinal LTS sub-models for biomarkers 1-3, survival sub-model, and variance-covariance matrix. The number of parameters in each parameter group can be read from the horizontal axis. The 4 curves demonstrate the percent bias (drawn to the vertical axis on the left) and relative efficiency (drawn to the vertical axis on the right) of each estimated parameter from the EM algorithm, under the sample size of $n = 300$ or $n = 1,000$. The relative efficiency is measured by the ratio of the empirical standard deviations of the point estimators from the EM and CCA. Values less than 1 indicate that EM is more efficient than CCA; smaller values indicate more efficiency improvement.*

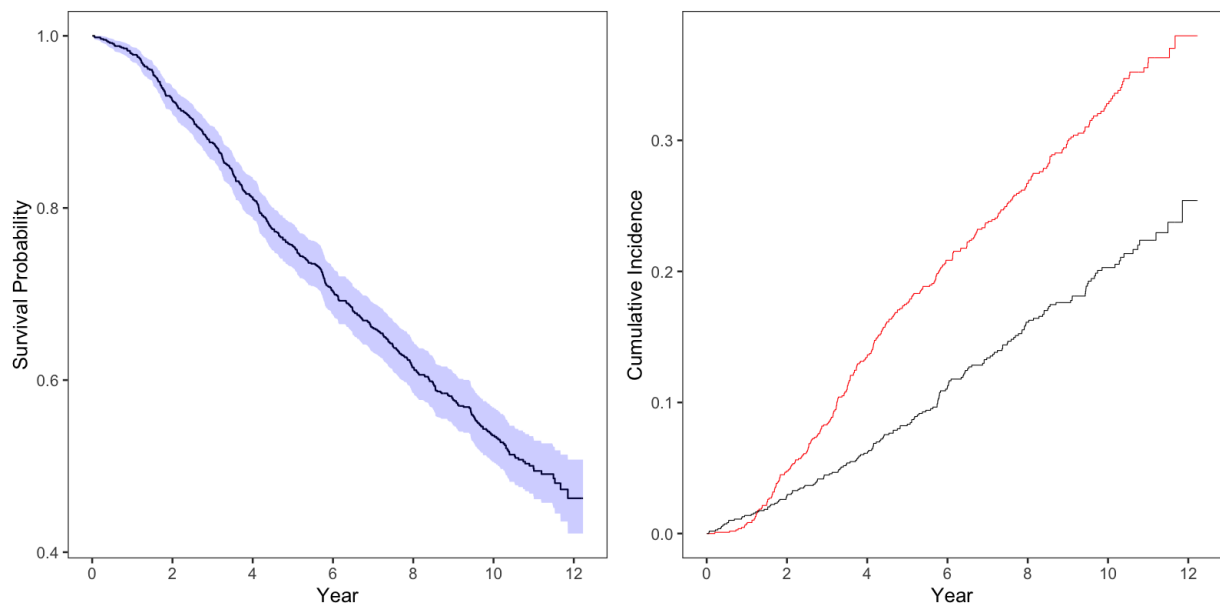


Figure 2: The Kaplan-Meier survival curve of the composite event of ESRD and death in the AASK study on the left and the cumulative incidence functions of ESRD (red) and death (black) on the right.

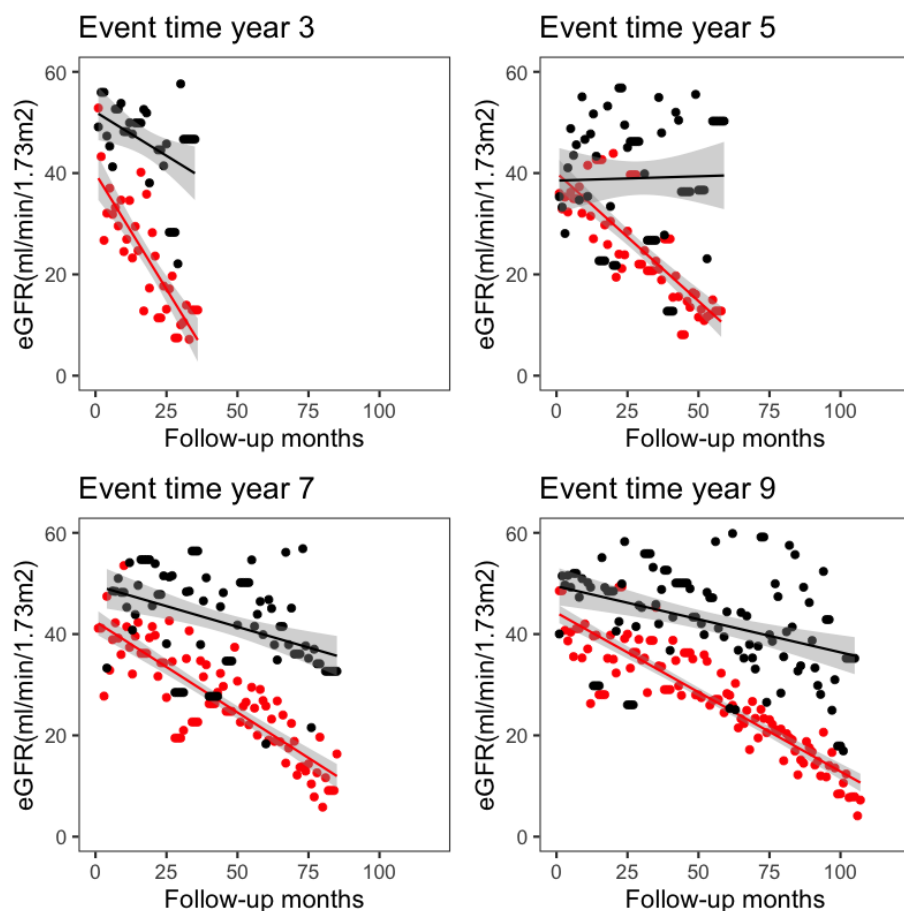


Figure 3: *The conditional mean trajectory (CMT) of eGFR at 4 selected composite event times in the AASK study. In each plot, we aggregated the longitudinal biomarker data from all subjects who had ESRD (red) or death (black) in that year. The dots show the mean biomarker by month, averaged across all subjects who had a measurement at that month. When the measurement times are non-informative, these biomarker means are unbiased estimators of the CMT at each month. A linear model is fitted to the monthly mean biomarker data for those with ESRD and death separately, with pointwise confidence intervals shown as gray bands.*

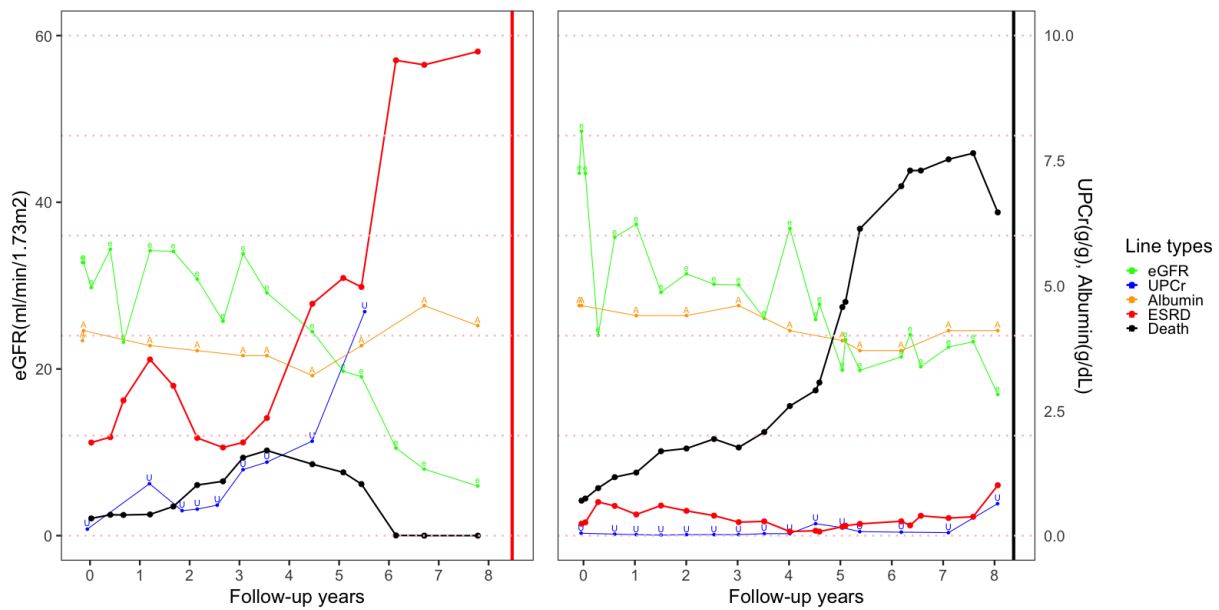


Figure 4: *Illustrating the dynamic prediction of ESRD and death with two AASK patients (patient A on the left and patient B on the right). The horizontal axis is the year since baseline. The longitudinal measurements of eGFR (green dots; connected by segments to form a continuous trajectory curve) are drawn to the vertical axis on the left; the longitudinal measurements of UPCr (blue dots and curve) and albumin (orange dots and curve) are drawn to the vertical axis on the right. The six horizontal dotted lines in the background mark the probability of 0, 0.2, 0.4, 0.6, 0.8, and 1.0, from bottom to the top. The predicted probabilities of ESRD (red dots; connected by linear segments to form a continuous curve) and death (black dots and curve) within a horizon of 3 years can be read from their positions among these six lines. The vertical red line marks the ESRD time of patient A; the vertical black line marks the death time of patient B. This dynamic prediction plot visualizes how the personalized, real-time risks of ESRD and death vary with the three longitudinal biomarkers. The prediction also incorporated baseline predictors.*

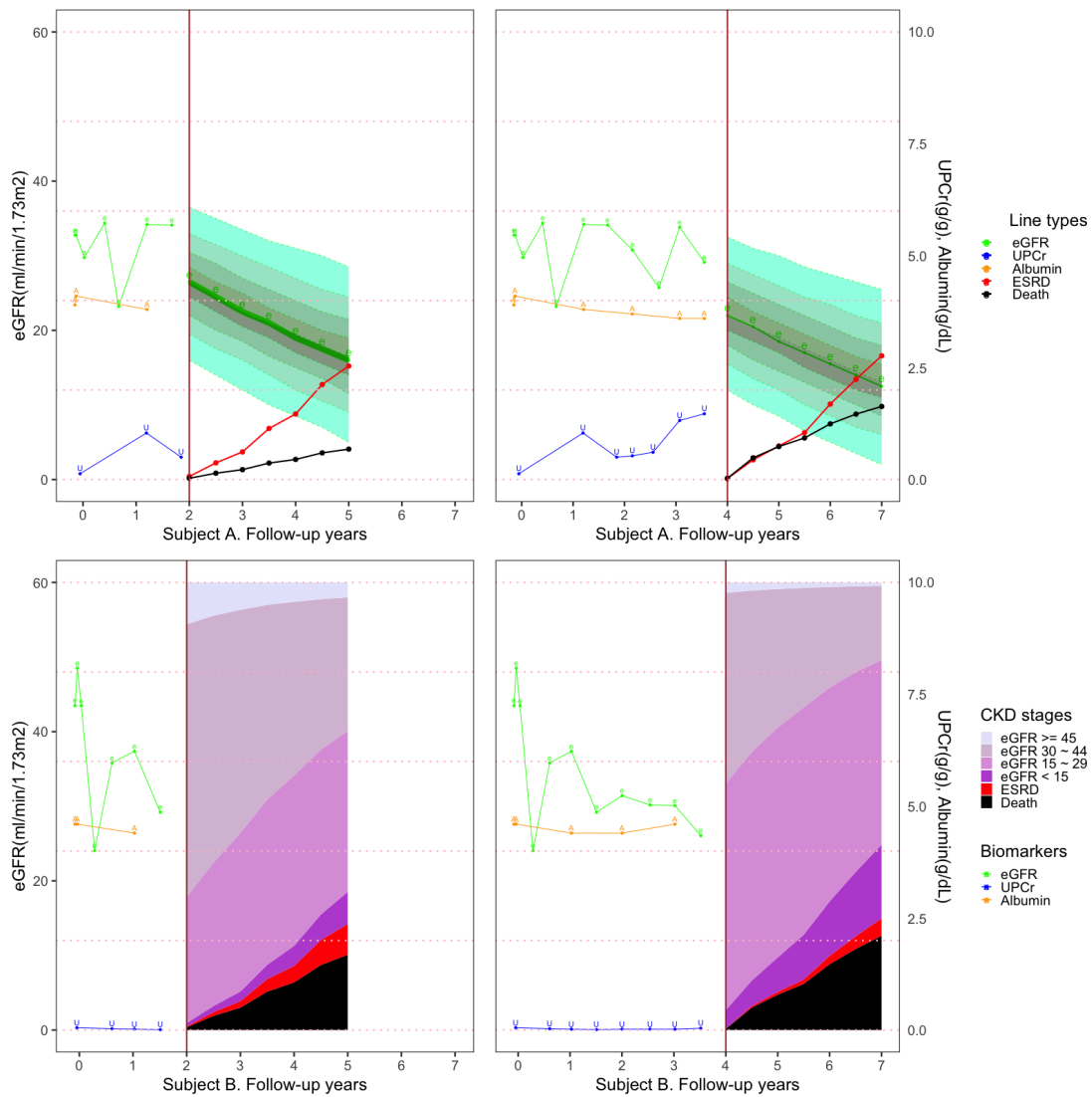


Figure 5: *Illustrating the joint prediction of the future ESRD, death and eGFR distributions in two graphical presentations. The top plots show the prediction of AASK patient A at two prediction times (vertical brown line), based on the accumulating biomarker history to the left. The bottom plots show patient B. These are the same two patients in Figure 4 and the plotting symbols are similar. The horizon is 3 years. With patient A, we plotted the predicted probabilities at 8 equally spaced future time points ($t = 0, 0.5, 1.0, \dots, 3.0$). At each time, we calculated the density function of eGFR and its 9 quantiles (10%, ..., 90%). These quantiles are plotted to the vertical axis on the left. For better visualization, we colored the areas between adjacent quantile curves into 8 green shaded areas. The thick green curve in the middle indicates the predicted mode of eGFR. With patient B, we plotted the multistate representation of all predicted outcomes (Hu et al., 2012). The probabilities of death, ESRD and CKD stages (defined by eGFR; see Section 1) were calculated up to the horizon. These probabilities were drawn to the dotted horizontal lines in the background, and they sum up to 1 at each time point.*

Table 1: Prediction accuracy results of BJM and SJM in the AASK data analysis. The prediction accuracy was evaluated among at-risk subjects at Year 1-4 after baseline. The prediction horizon is 3 years. SJM: shared random effects joint model.

Accuracy	Type	Model	Year1	Year2	Year3	Year4
AUC	ESRD	BJM-3-TP	0.9068	0.9378	0.9267	0.9008
AUC	ESRD	BJM-2-TP	0.9068	0.9358	0.9259	0.8987
AUC	ESRD	BJM-1-TP	0.8727	0.9135	0.9322	0.9135
AUC	ESRD	BJM-3-EX	0.9057	0.9398	0.9342	0.9182
AUC	ESRD	BJM-2-EX	0.9096	0.9492	0.9527	0.9587
AUC	ESRD	BJM-1-EX	0.8796	0.9314	0.9358	0.9277
AUC	ESRD	SJM-3	0.8941	0.8945	0.9506	0.9449
AUC	Death	BJM-3-TP	0.7354	0.6430	0.6736	0.6725
AUC	Death	BJM-2-TP	0.7083	0.6099	0.6569	0.6620
AUC	Death	BJM-1-TP	0.6586	0.6387	0.6162	0.5888
AUC	Death	BJM-3-EX	0.5999	0.6554	0.6403	0.6295
AUC	Death	BJM-2-EX	0.5873	0.6114	0.6098	0.6163
AUC	Death	BJM-1-EX	0.6242	0.6497	0.6605	0.6566
AUC	Death	SJM-3	0.6709	0.6316	0.6243	0.6874
BS	ESRD	BJM-3-TP	0.0672	0.0585	0.0677	0.0714
BS	ESRD	BJM-2-TP	0.0659	0.0586	0.0677	0.0710
BS	ESRD	BJM-1-TP	0.0776	0.0690	0.0652	0.0672
BS	ESRD	BJM-3-EX	0.0686	0.0582	0.0673	0.0693
BS	ESRD	BJM-2-EX	0.0677	0.0640	0.0739	0.0809
BS	ESRD	BJM-1-EX	0.0809	0.0786	0.0812	0.0921
BS	ESRD	SJM-3	0.1177	0.1151	0.1078	0.0718
BS	Death	BJM-3-TP	0.0422	0.0512	0.0642	0.0748
BS	Death	BJM-2-TP	0.0425	0.0514	0.0646	0.0741
BS	Death	BJM-1-TP	0.0422	0.0486	0.0588	0.0674
BS	Death	BJM-3-EX	0.0442	0.0504	0.0614	0.0710
BS	Death	BJM-2-EX	0.0550	0.0699	0.0878	0.1020
BS	Death	BJM-1-EX	0.0547	0.0694	0.0868	0.1009
BS	Death	SJM-3	0.0867	0.1081	0.1279	0.1306
RMSE	eGFR	BJM-3-TP	8.1559	8.7276	8.4907	8.2903
RMSE	eGFR	BJM-3-EX	10.6981	10.6853	9.5622	8.4871
RMSE	eGFR	SJM-3	8.8914	8.9091	8.0943	6.8213
P30	eGFR	BJM-3-TP	0.9156	0.9241	0.9469	0.9308
P30	eGFR	BJM-3-EX	0.7891	0.8254	0.8607	0.9000
P30	eGFR	SJM-3	0.9213	0.9195	0.9110	0.9466
P50	eGFR	BJM-3-TP	0.9600	0.9709	0.9812	0.9853
P50	eGFR	BJM-3-EX	0.9553	0.9520	0.9614	0.9742
P50	eGFR	SJM-3	0.9683	0.9831	0.9874	0.9871
# at-risk patients in AASK data			1065	1005	955	875